Article

Journal of Nanoscience and Nanotechnology
Vol. 20, 3823–3831, 2020
www.aspbs.com/jnn

Quenching Assisted Reverse Micellar Synthesis and Electrical Properties of High Surface Area $BiFeO_3$ Nanoparticles

Irfan H. Lone[1,2], Abul Kalam[3], Jahangeer Ahmed[4], Norah Alhokbany[4], Saad M. Alshehri[4], and Tokeer Ahmad[1,*]

[1] Nanochemistry Laboratory, Department of Chemistry, Jamia Millia Islamia, New Delhi 110025, India
[2] Department of Chemistry, College of Science, Taibah University, Yanbu-30799, Al-Madina, Saudi Arabia
[3] Department of Chemistry, Faculty of Science, King Khalid University, Abha 61413, Saudi Arabia
[4] Department of Chemistry, College of Science, King Saud University, Riyadh 11451, Saudi Arabia

Multiferroic compounds are prime important materials for future electronic and magnetic devices and overcome the fundamental limits of conventional materials. In present work, we reported the preparation of purely one phase of nano-sized $BiFeO_3$ compound by microemulsion micellar method for the first time by employing rapid quenching of sample at 500 °C, that is the main driving force to get the pure phase of $BiFeO_3$ nanoparticles at low temperature method. The nanoparticles that we obtained were almost uniform with sphere shaped and these prepare nanoparticles possess high surface. The increase in permittivity in the form of dielectric constants were reported that depends on temperature and frequency that supports the ferroelectric nature and was further confirmed by the ferroelectric loops even at the room temperature has been found in theses prepared nanoparticles.

Keywords: Nanoparticles, Reverse Micelles, Quenching, Bismuth Ferrite, Surface Area, Ferroelectricity.

1. INTRODUCTION

In recent time, an adequate importance and research focus have been given to the multiferroic materials as they possess multidimensional properties that have been utilized in the device fabrications [1–4]. Such kind of materials has advance applications in future computers memory devices, sensors and in actuators and transducers [5]. Recently, few multifunctional nanostructures showed their extensive applications in photo/electro catalytic water splitting, gas sensor, dye degradation and super-capacitors [6–8]. However, multiferroic $BiFeO_3$ is selectively used in telecommunications such as radio, TV and recording devices like chips, digital devices and so on [9]. Bismuth ferrite nanoparticles used in ferroelectric memory switching devices due to the control of leakage current and better ferroic properties [10, 11]. Among ferroelectric materials, bismuth ferrite based photovoltaic solar cells has shown high power conversion efficiency due to its visible band gap in the range of 2.1 to 2.7 eV [12, 13]. The low cost cells that has been used in solar devices were ecofriendly and green reservoir of energy and it was first time reported on Dye-sensitized solar cells (DSSCs) prepared by use of $BiFeO_3$ nanowires [14]. The band gap of $BiFeO_3$ compound lie in the visible range and constitutes a great material for the possible penetration of $BiFeO_3$ nanoparticles in projecting functioning in dye sensitized solar cells and in photovoltaic widgets. These semiconductor materials that absorb the light in visible range possess eminent properties in chemical stable order, electron moving quality and the degree of being harmless [15–18] and came up with effective photo catalyst [19–22]. In addition, the ferroic nature of $BiFeO_3$ assists in recycling photo catalysts after use in reaction by an external magnetic field prevents the loss of catalysts, and makes cost effective catalyst and this peculiar property the photocatalytic behavior of $BiFeO_3$ has been explored previously [23–26].

*Author to whom correspondence should be addressed.

The synthesis of $BiFeO_3$ nanoparticles have considered as a challenge because of the other secondary phases that includes $Bi_{25}FeO_{39}$ and $Bi_2Fe_4O_9$. The solid-state synthesis in the temperature range of 800–830 °C from Bi_2O_3 and Fe_2O_3 is tough to reproduce the product [27]. The low temperature synthesis methods prevent the appearance of secondary phases and the synthesized $BiFeO_3$ found to have enhanced magnetic, ferroelectric and dielectric properties [28–30]. The varieties of metal and metal oxides synthesized via polymeric citrate precursor, reverse micelle and solvothermal routes without using any costly equipment [31–35]. There was not any reverse micellar type method reported for the preparation of $BiFeO_3$ nanoparticles. The attraction of this method lies in the fact that it possesses micellar nanoreactor where the size of prepared nanoparticles can have controlled with controlling ratio of surfactant and water molecule [36].

2. EXPERIMENTAL DETAILS

0.1 M concentration solution of bismuth nitrate, iron nitrate, and ammonium oxalate monohydrate respectively synthesized in the double distilled water. For three microemulsions preparation, there needs two metal ions respectively for I and II microemulsion and one precipitation agent for the III microemulsion. Additionally, it requires surfactant tergitol NP-9 of 21 ml and 1-octanol of 15.6 ml as cosurfactant and non-polar solvent 180 ml cyclohexane. The two metal ions microemulsion were mixed and stirred 2 hours, after that added third precipitating microemulsion and again stirred for 2 hours. Then the whole microemulsion was heated at 60 ± 5 °C and reddish brown precipitates was found in the reaction vessel. The product obtained after centrifuging was washed and was then calcined at 500 °C for 2 hours, thereafter was quenched to room temperature which is very important step for the preparation of monophasic of $BiFeO_3$ nanoparticles. The whole procedure is shown in the form of flow chart given in the Figure 1.

Using Bruker D8 Advance the powder diffraction was held having radiations of Cu-Kα having wavelength (λ) of 1.54056 Å. The complete diffraction scan have been recorded 10° to 70° 2θ range with 0.05° step size. Perkin-Elmer spectrometer has used for the study of Fourier transform infrared spectra (FT-IR). The thermogravimetric study TGA of synthesized nanoparticles was determined by Perkin-Elmer Diamond analyser with heating rate of 10 °C min^{-1} in between temperature range of 30 °C

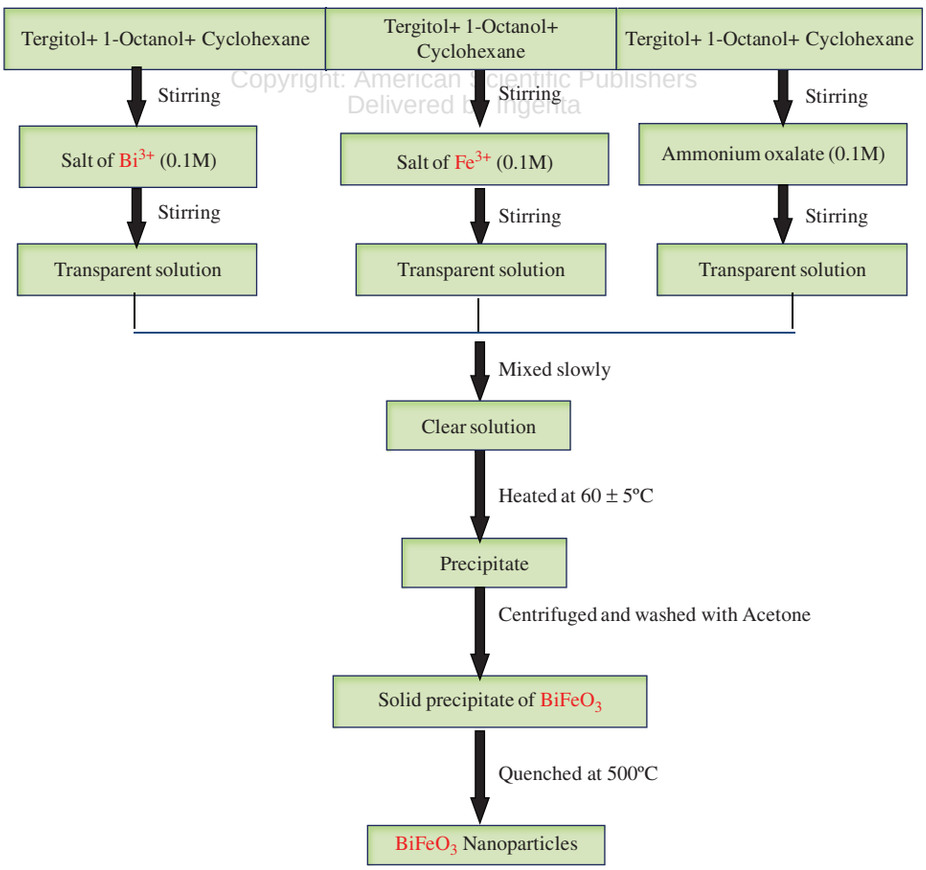

Figure 1. Flow chart for the synthesis of $BiFeO_3$ nanoparticles using reverse micelles.

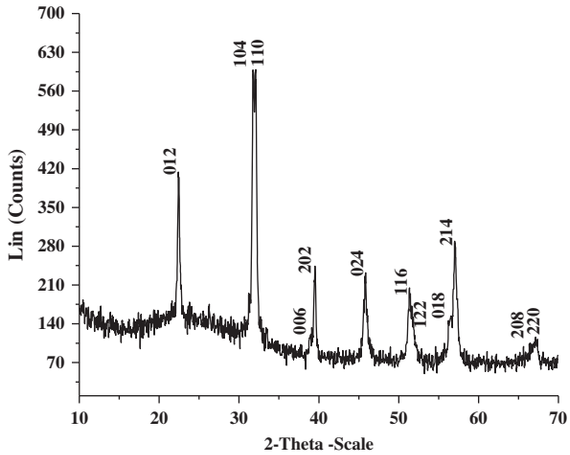

Figure 2. Powder X-ray diffraction pattern of $BiFeO_3$ nanoparticles.

to 900 °C. Microscopic pictures were taken by the use of transmission electron microscopic and scanning electron microscopic on FEI Tecnai G^2 20 TEM and ZEISS EVO 50 SEM machines respectively. Surface properties

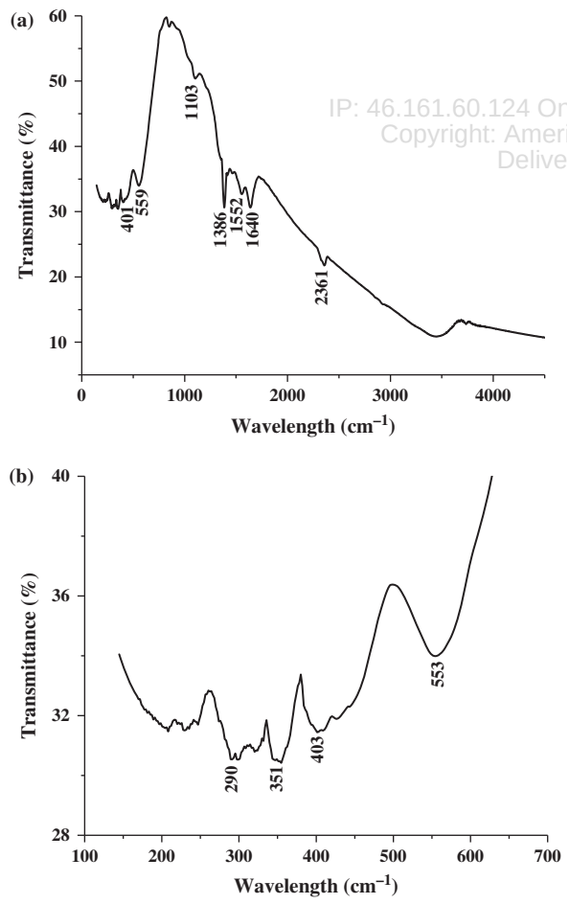

Figure 3. FTIR spectra of $BiFeO_3$ nanoparticles (a) before and (b) after calcination.

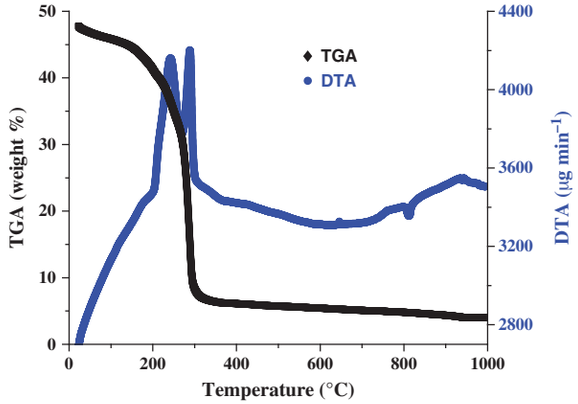

Figure 4. TGA and DTA graphs of $BiFeO_3$ nanoparticles.

of prepared sample were checked using Quantachrome, Nova 2000e Instrument BET machine at 77 K of liquid nitrogen temperature. Spectrophometer double beamed Perkin-Elmer Lamda-35 used to find out the band gap

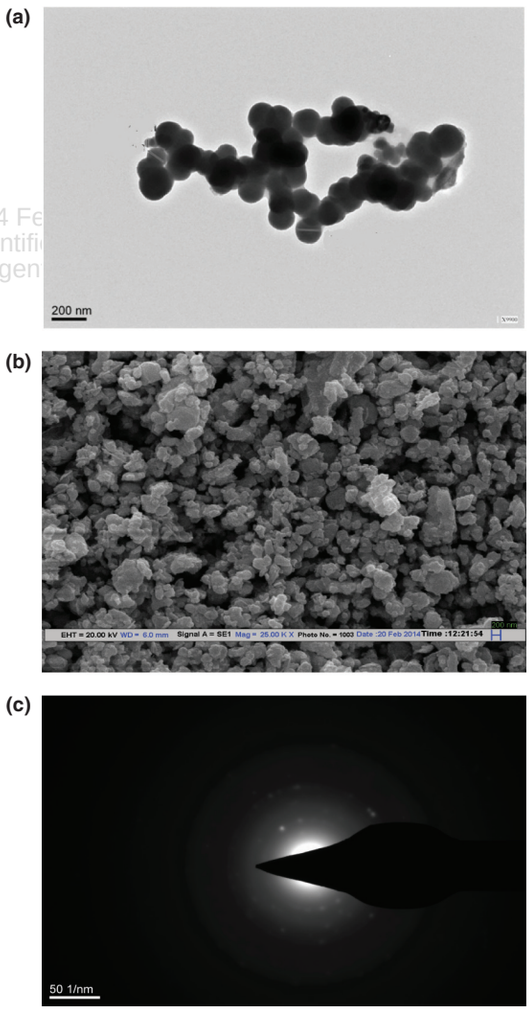

Figure 5. (a) TEM, (b) SEM and (c) SAED micrographs of as-prepared $BiFeO_3$ nanoparticles.

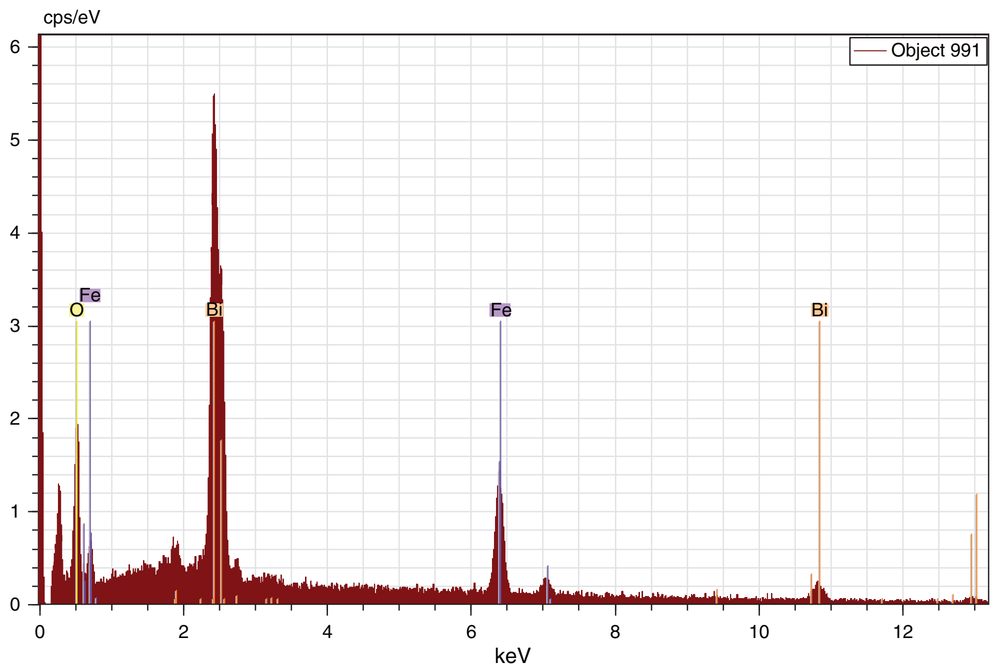

Figure 6. EDAX spectra of $BiFeO_3$ nanoparticles.

in the reflection mode. Small amount of $BaSO_4$ as reference works for the reflectance spectra and band gap of nanoparticles was found by calculation of Kubelka-Munk function $F(R)$ [37, 38] by the use of famous equation $F(R) = (1-R)^2/2R$.

In case of dielectric study, 10 mm diameter pellet has been prepared by gridding and then mixing polyvinyl alcohol aqueous solution. The slurry was the dried, pressed at a pressure of 5 tons and then painted with colloidal silver on the both faces of pellet before annealing. Using HF LCR meter, the dielectric properties measured in frequency range 100 kHz to 2 MHz in presence of temperature from 50 °C to 450 °C. Lastly the *P–E* (room temperature) ferroelectricity study was found by the *P–E* loop tracer radiant USA instrument.

3. RESULTS AND DISCUSSION

Single phase and structure of prepared $BiFeO_3$ nanoparticles checked out by diffraction technique. Complete reflection peaks indexed with hexagonal structure of $BiFeO_3$ (JCPDS 71-2494) shown in Figure 2 and FTIR spectra shown in Figures 3(a), (b) needed to characterize before and after calcinations. Capping molecules on $BiFeO_3$ nanoparticles like surfactants and co-surfactants has been confirmed in the Figure 3(b) and the band value of 553 cm^{-1} and other low band values wave numbers suggested the presence of (Fe–O) bonds and this part of explanation was proved earlier in Fe_3O_4 compound [39]. Temperature variation effect on $BiFeO_3$ nanoparticles was figured by the employ of TGA-DTA depicted in the Figure 4. From the graph of TGA the initial deprivation in weight close to 200 °C may due to water evaporation and water adsorption on nanoparticles. Thenceforth deprivation at 300 °C may be associated with excretion of organic compounds like surfactants and cosurfactants, this kind of result was further backed by the existence of two exothermic peaks in DTA diagram. Then after there could not find any decline in the weight that confirms the stability of prepared nanoparticles with temperature. The XRD studies of $BiFeO_3$ nanoparticles at 500 °C also support the thermal stability investigations of thermogravimetric studies.

To investigate the grain size, transmission electron microscopy has been employed to get the images of prepared $BiFeO_3$ nanoparticles. Crystalline nature and morphology of prepared samples were confirmed and further analysed with the help of scanning microscope and electron diffraction techniques SEM and SAED respectively. TEM and SEM images of $BiFeO_3$ nanoparticles show the formation of spherical shaped particles having 80 nm, small size distribution given in Figures 5(a) and (b). The size of 80 nm using microscopic images like TEM/SEM was found smaller than crystallite size of 96 nm getting from Scherrer's studies. The size obtained by XRD is not accessible for the powdered samples as the XRD studies are more favorable for single crystal. In case of powdered samples, the several crystallites that are fused by small angle boundaries with different degree of orientations are associated with the fact that the crystallites diffract separately in XRD. There are other defects like lattice strain or micro-strain is a local deviation of *d*-spacings from the

average value, caused by local defects. SAED kind of electron diffraction of $BiFeO_3$ nanoparticles in the Figure 5(c) was found pointed spots, hence indicates actual preparation of nano $BiFeO_3$ particles. The atomic ratio 1:1 with respect to Bi and Fe elements was found in the elemental detection analysis that shows the sample prepared was very close to the loaded composition and this EDAX analysis was shown in Figure 6. Hence it was proved that stoichiometric ratio of $BiFeO_3$ elements was respectively the same without any impurity.

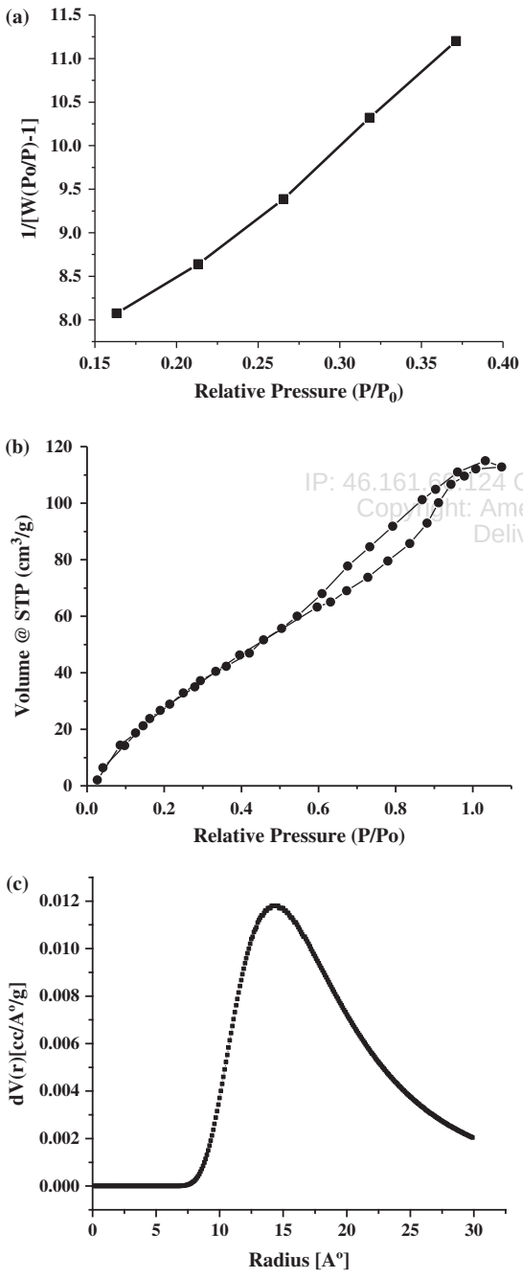

Figure 7. (a) BET, (b) N_2 adsorption isotherm and (c) DA plots of $BiFeO_3$ nanoparticles.

BET surface area adsorption method used to determine the surface area of as-prepared $BiFeO_3$ nanoparticles. For specific surface area, the linearity range was restricted upto 0.05–0.30 value. Surface area of 205 m^2g^{-1} was achieved of $BiFeO_3$ nanoparticles given Figure 7(a) and this value of surface area was much better than the previously reported so far [40, 41]. N_2 adsorption–desorption isotherm of $BiFeO_3$ nanoparticles (Fig. 7(b)) shows the type IV curve that matches with H1-type hysteresis (according to the isotherm classification), that are related to cylindrical pores of mesoporous materials. The DA plot as shown in Figure 7(c) confirms the pore radius of 14.3 Å.

Light properties of $BiFeO_3$ nanoparticles were studied at room temperature in the ultra violet and visible portion for getting the reflectance spectra. Value of the band gap got from the plot of $[F(R) \cdot E_g]^2$ against (E_g) of nanoparticles $BiFeO_3$ given in Figure 8. By extrapolating graph $(F(R) \cdot E_g)^2$ versus E_g to point that touches to y-axis at zero gives the band gap and was thus determined at an around ∼2.12 eV for $BiFeO_3$ nanoparticles that actually matches in visible portion of electromagnetic radiation and that may help in degradation of organic dyes present in water. The narrowest visible band gap of ∼2.12 eV indicates that high power conversion efficiency may be obtained by $BiFeO_3$ based photovoltaic solar cells.

The dielectric properties like dielectric constant, loss data values deviate with different frequency keeping temperature constant at room temperature as shown in Figure 9(a). The dielectric parameters as usual decrease by the rise of frequency and matches with Maxwell-Wagner type interfacial polarization [42, 43] that also agrees theory of Koop's phenomenological law [44]. The dielectric constant 67.6 and dielectric loss 0.15 values of prepared nanoparticles at room temperature was reported respectively in presence of 500 kHz frequency. In the second case, the change of dielectric properties by the change of temperature at constant frequency of 1 MHz was shown

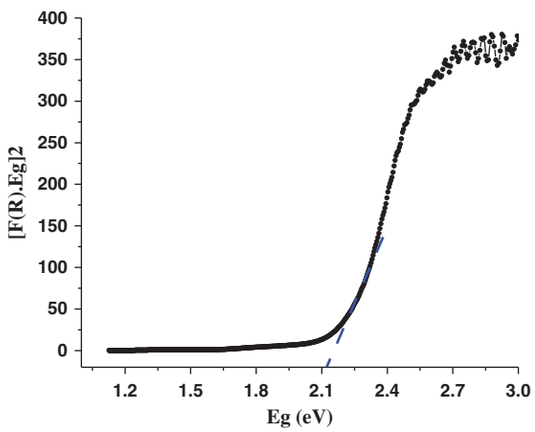

Figure 8. Band gap plot of $BiFeO_3$ nanoparticles.

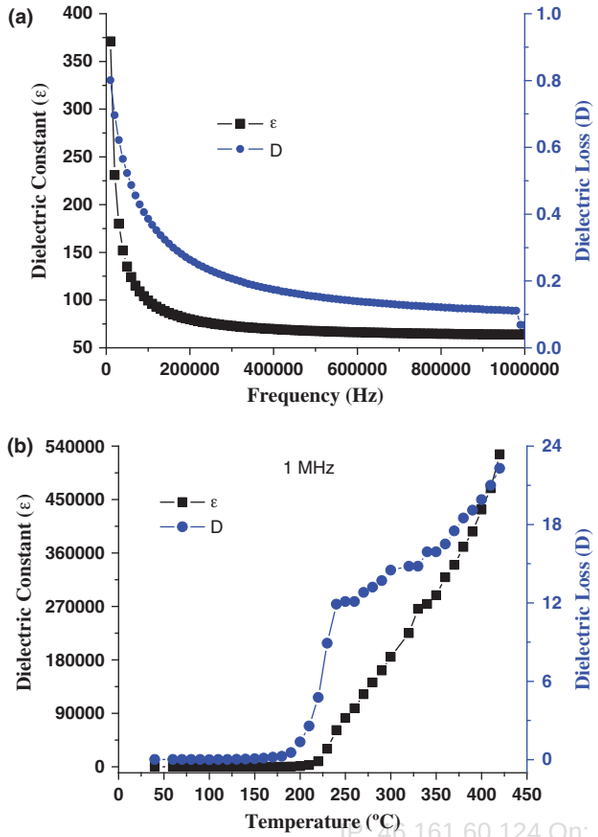

Figure 9. The variation of dielectric constant and dielectric loss of $BiFeO_3$ nanoparticles as a function of (a) frequency and (b) temperature.

in Figure 9(b). The dielectric characteristics remain stable at 200 °C temperature and after that phase transition high dielectric values have been observed just like in ferroelectric oxide materials. In temperature between 200–250 °C, the peak can be considered anti-ferromagnetic (T_N) phase transition temperature of $BiFeO_3$ nanoparticles that could be suggested that there is a quite relational between the effect of magnetic and electric field presence and this value of Neel temperature was lower than bulk $BiFeO_3$ (337 °C) [45]. In the case of another perceptive dielectric loss study possess the almost same variation with frequency and temperature. Dipole contribution in the polarization at high frequency decreases the dielectric loss [46]. The very low values of dielectric loss up to 200 °C (Fig. 9(b)) indicates that prepared sample is better insulator as was expected for good quality $BiFeO_3$ material [47, 48]. The temperature dependence of dc conductivity of $BiFeO_3$ nanoparticles was plotted using Arrhenius equation: $\sigma = \sigma_0 \exp(-E_{\text{cond}}/(k_B T))$, here σ_0 pre-exponential condition and E_{cond} conduction activation energy. This activation conduction energy (E_{cond}) estimated by the slope of $\log \sigma_{\text{dc}}$ against 1000 T^{-1} K as shown in Figure 10. The activation energy value using Figure 10 has been observed 0.324 eV. This indicates that the hopping mechanism of conducting ions of $BiFeO_3$ nanoparticles involved for conduction behaviour and also

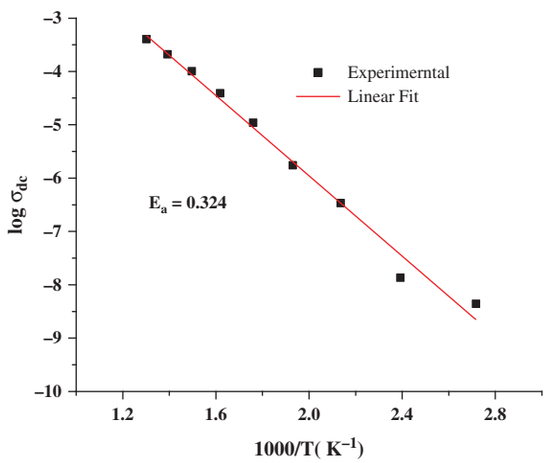

Figure 10. Arrhenius plot of $BiFeO_3$ nanoparticles. The symbols are experimental points and the solid line is Arrhenius fit.

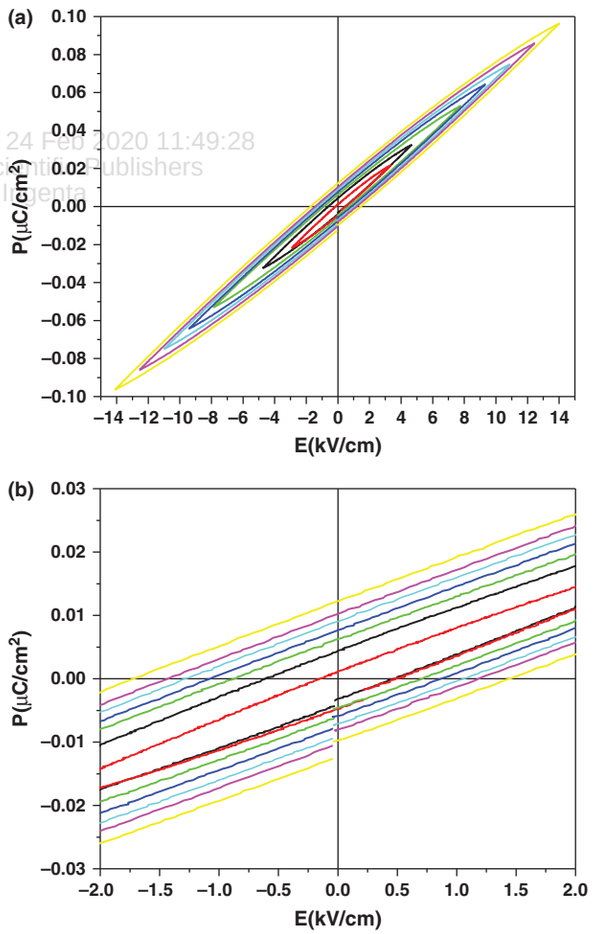

Figure 11. (a) Full and (b) closer view of the *P*–*E* hysteresis loops of $BiFeO_3$ nanoparticles.

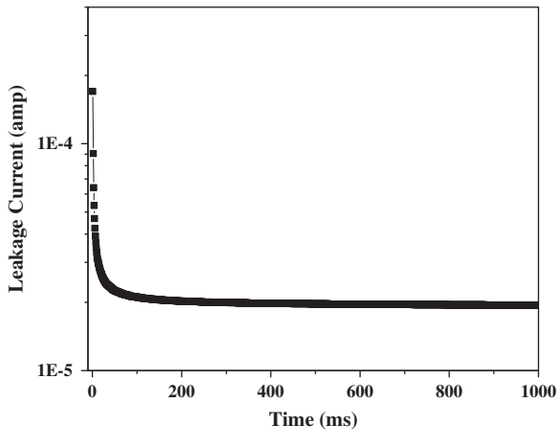

Figure 12. Variation of leakage current data as a function of time for $BiFeO_3$ nanoparticles.

resembles with the value of semi-conductive ferroelectric materials [49].

One more interesting results of polarization versus electric field hysteresis have been observed for the prepared nanoparticles at various applied voltages and these results were achieved in 50 kHz frequency. These ferroelectric loop properties of $BiFeO_3$ nanoparticles after sintered pellet at 600 °C are all given in Figures 11(a), (b). The data values of 0.096 $\mu C/cm^2$, 0.012 $\mu C/cm^2$ and 1.7 $kVcm^{-1}$ respectively of saturation, remanent and coercive field were obtained by applying the voltage of 900 volt. If the applied voltage has been decreased it was observed that the data values also decreased and also affects the area of the hysteresis loop. This means that area of the loop and these parameters are very sensitive on the applied voltage. The second important analysis was noticed that after sintering more than 600 °C temperature there were no significant hysteresis loop and could be related with leakage current shown in Figure 12. Solid electrolytic capacitors have this type of behaviour and improved resistivities that were found in $BiFeO_3$ nanoparticles is because of different sizes of grains that helps and promotes the loss of current and may provide the conduction pathways. Hence for the narrow size distribution as found in the present study led for the little leaky current and better resistivity.

4. CONCLUSION

High surface-area mesoporous nanostructured $BiFeO_3$ without the formation of undesirable phase was first time reported using reverse micellar route. XRD and FTIR techniques proves the non-presence of secondary or impurity phases in the prepared sample. Electron microscopic images and diffraction reveals the nanocrystalline nature and N_2 physisorption results of $BiFeO_3$ nanoparticles confirm the high surface area and pore radius lies in the mesopore range. The visible band gap for $BiFeO_3$ nanoparticles suggests that it may be applied in photovoltaic solar cells with high power conversion efficiency. Room temperature polarization electric field hysteresis loop in prepared $BiFeO_3$ nanoparticles was found with reasonably good loop parameter values. The electrical characterization (dielectric properties, conductivity and impedance) of the prepared sample at variable frequencies function of the temperature range were obtained and has shown that the prepared nanoparticles are better insulator for the desired quality of $BiFeO_3$ material.

Acknowledgments: The authors thank AIIMS Delhi for microscopic studies, CIF Jamia Millia Islamia for X-ray diffraction studies and Dr. V. R. Reddy, UGC-DAE Indore for *P–E* loop studies. Tokeer Ahmad thanks to SERB-DST New Delhi, Gov. of India for financial support to the research scheme No. EMR/2016/001668. Irfan H. Lone thanks to UGC Delhi for the (JRF and SRF) fellowship. The authors extend their sincere appreciation to Researchers Supporting Project Number (RSP-2019/29), King Saud University, Riyadh, Saudi Arabia for funding this research. The author (Abul Kalam) extends their appreciation to the Deanship of Scientific Research at King Khalid University for funding this work through research groups program under grant number RGP 1/49/39.

References and Notes

1. Newnham, R.E., **2004**. The amplitude-frequency effect in quartz resonators. *Ferroelectrics, 306*(1), pp.211–220.
2. Ahmad, T. and Lone, I.H., **2016**. Citrate precursor synthesis and multifunctional properties of $YCrO_3$ nanoparticles. *New Journal of Chemistry, 40*(4), pp.3216–3224.
3. Shokrollahi, H., **2009**. The magnetic and structural properties of the most important alloys of iron produced by mechanical alloying. *Mater. Design, 30*(9), pp.3374–3387.
4. Ahmad, T., Lone, I.H. and Ubaidullah, M., **2015**. Structural characterization and multiferroic properties of hexagonal nanosized $YMnO_3$ developed by low temperature precursor route. *RSC Advances, 5*(1), pp.58065–58071.
5. Fiebig, M., Lottermoser, T., Frohlich, D., Goltsev, A.V. and Pisarev, R.V., **2002**. Observation of coupled magnetic and electric domains. *Nature, 419*(6909), pp.818–820.
6. Ahmad, T., Lone, I.H., Ansari, S.G., Ahmed, J., Ahamad, T. and Alshehri, S.M., **2017**. Multifunctional properties and applications of yttrium ferrite nanoparticles prepared by citrate precursor route. *Materials & Design, 126*, pp.331–338.
7. Ahmad, T., Phul, R., Alam, P., Lone, I.H., Shahazad, M., Ahmed, J., Ahamad, T. and Alshehri, S.M., **2017**. Dielectric, optical and enhanced photo-catalytic properties of $CuCrO_2$ nanoparticles. *RSC Advances, 7*(44), pp.27549–27557.
8. Alshehri, S.M., Ahmed, J., Ahamad, T., Arunachalam, P., Ahmad, T. and Khan, A., **2017**. Bifunctional electro-catalytic performances of $CoWO_4$ nanocubes for water redox reactions (OER/ORR). *RSC Advances, 7*(72), pp.45615–45623.
9. Cheong, S.W. and Mostovoy, M., **2007**. Multiferroics: A magnetic twist for ferroelectricity. *Nature Materials, 6*(1), pp.13–20.

10. Yang, C.H., Seidel, J., Kim, S.Y., Rossen, P.B., Yu, P., Gajek, M., Chu, Y.H., Martin, L.W., Holcomb, M.B., He, Q. and Maksymovych, P., **2009**. Electric modulation of conduction in multiferroic Ca-doped $BiFeO_3$ films. *Nature Materials, 8*(6), pp.485–493.
11. Luo, J.M., Lin, S.P., Zheng, Y. and Wang, B., **2012**. Nonpolar resistive switching in Mn-doped $BiFeO_3$ thin films by chemical solution deposition. *Applied Physics Letters, 101*(6), p.062902.
12. Chen, G., Chen, J., Pei, W., Lu, Y., Zhang, Q., Zhang, Q. and He, Y., **2019**. Bismuth ferrite materials for solar cells: Current status and prospects. *Materials Research Bulletin, 110*, pp.39–49.
13. Loh, L., Briscoe, J. and Dunn, S., **2016**. Bismuth ferrite enhanced ZnO solid state dye-sensitised solar cell. *Procedia Engineering, 139*, pp.15–21.
14. Lotey, G.S. and Verma, N.K., **2014**. Synthesis and characterization of $BiFeO_3$ nanowires and their applications in dye-sensitized solar cells. *Materials Science in Semiconductor Processing, 21*, pp.206–211.
15. Catalan, G. and Scott, J.F., **2009**. Physics and applications of bismuth ferrite. *Advanced Materials, 21*(24), pp.2463–2485.
16. Huo, Y., Jin, Y. and Zhang, Y., **2010**. Citric acid assisted solvothermal synthesis of $BiFeO_3$ microspheres with high visible-light photocatalytic activity. *Journal of Molecular Catalysis A: Chemical, 331*(1–2), pp.15–20.
17. Joshi, U.A., Jang, J.S., Borse, P.H. and Lee, J.S., **2008**. Microwave synthesis of single-crystalline perovskite $BiFeO_3$ nanocubes for photoelectrode and photocatalytic applications. *Applied Physics Letters, 92*(24), p.242106.
18. Gao, F., Chen X.Y., Yin, K.B., Dong, S., Ren, Z.F., Yuan, F., Yu, T., Zou, Z.G. and Liu, J.M., **2007**. Visible light photocatalytic properties of weak magnetic $BiFeO_3$ nanoparticles. *Advanced Materials, 19*(19), pp.2889–2892.
19. Wei, J., Zhang, C. and Xu, Z., **2012**. Low-temperature hydrothermal synthesis of $BiFeO_3$ microcrystals and their visible-light photocatalytic activity. *Materials Research Bulletin, 47*(11), pp.3513–3517.
20. Lotey, G.S. and Verma, N.K., **2013**. Gd-doped $BiFeO_3$ nanoparticles—A novel material for highly efficient dye-sensitized solar cells. *Chemical Physics Letters, 574*, pp.71–77.
21. Lotey, G.S. and Verma, N.K., **2013**. Phase-dependent multiferroism in Dy-doped $BiFeO_3$ nanowires. *Superlattices and Microstructures, 53*, pp.184–194.
22. Lotey, G.S. and Verma, N.K., **2013**. Multiferroic properties of Tb-doped $BiFeO_3$ nanowires. *Journal of Nanoparticle Research, 15*(4), pp.1553–1.
23. Papadas, I.T., Subrahmanyam, K.S., Kanatzidis, M.G. and Armatas, G.S., **2015**. Templated assembly of $BiFeO_3$ nanocrystals into 3D mesoporous networks for catalytic applications. *Nanoscale, 7*(13), pp.5737–5743.
24. Bharathkumar, S., Sakar, M. and Balakumar, S., **2016**. Experimental evidence for the carrier transportation enhanced visible light driven photocatalytic process in bismuth ferrite ($BiFeO_3$) one-dimensional fiber nanostructures. *The Journal of Physical Chemistry C, 120*(33), pp.18811–18821.
25. Zhang, J., Huang, Y., Jin, L., Rosei, F., Vetrone, F. and Claverie, J.P., **2017**. Efficient upconverting multiferroic core@shell photocatalysts: Visible-to-near-infrared photon harvesting. *ACS Applied Materials and Interfaces, 9*(9), pp.8142–8150.
26. Mohan, S., Subramanian, B. and Sarveswaran, G., **2014**. A prototypical development of plasmonic multiferroic bismuth ferrite particulate and fiber nanostructures and their remarkable photocatalytic activity under sunlight. *Journal of Materials Chemistry C, 2*(33), pp.6835–6842.
27. Achenbach, G.D., James, W.J. and Gerson, R., **1967**. Preparation of single-phase polycrystalline $BiFeO_3$. *Journal of the American Ceramic Society, 50*(8), pp.437–441.
28. Liu, J., Fang, L., Zheng, F., Ju, S. and Shen, M., **2009**. Enhancement of magnetization in Eu doped $BiFeO_3$ nanoparticles. *Applied Physics Letters, 95*(2), p.022511.
29. Guo, R., Fang, L., Dong, W., Zheng, F. and Shen, M., **2010**. Enhanced photocatalytic activity and ferromagnetism in Gd doped $BiFeO_3$ nanoparticles. *The Journal of Physical Chemistry C, 114*(49), pp.21390–21396.
30. Zhang, Y., Zhang, H., Yin, J., Zhang, H., Chen, J., Wang, W., Chen, J.L., Wang, W.Q. and Wu, G.H., **2010**. Structural and magnetic properties in $Bi_{1-x}R_xFeO_3$ ($x = 0$–1, R = La, Nd, Sm, Eu and Tb) polycrystalline ceramics. *Journal of Magnetism and Magnetic Materials, 322*(15), pp.2251–2255.
31. Ahmad, T. and Ganguli, A.K., **2006**. Structural and dielectric characterization of nanocrystalline $(Ba, Pb)ZrO_3$ developed by reverse micellar synthesis. *Journal of the American Ceramic Society, 89*(10), pp.3140–3146.
32. Ahmad, T., Wani, I.A., Ahmed, J. and Al-Hartomy, O.A., **2014**. Effect of gold ion concentration on size and properties of gold nanoparticles in tritonX-100 based inverse microemulsions. *Applied NanoScience, 4*(4), pp.491–498.
33. Ganguli, A.K., Ahmad, T., Arya, P.R. and Jha, P., **2005**. Nanoparticles of complex metal oxides synthesized using the reverse micellar and polymeric precursor routes. *Pramana, 65*(5), pp.937–947.
34. Ahmad, T., Khatoon, S., Coolahan, K. and Lofland, S.E., **2013**. Structural characterization, optical and magnetic properties of Ni-doped CdO dilute magnetic semiconductor nanoparticles. *Journal of Materials Research, 28*(9), pp.1245–1253.
35. Ahmad, T., Khatoon, S., Coolahan, K. and Lofland, S.E., **2013**. Solvothermal synthesis, optical and magnetic properties of nanocrystalline $Cd_{1-x}Mn_xO$ ($0.04 < x = 0.10$) solid solutions. *Journal of Alloys and Compounds, 558*, pp.117–124.
36. Shah, M.A. and Ahmad, T., **2010**. *Principles of Nanoscience and Nanotechnology*. Alpha Science International.
37. Kortum, G., **1969**. *Reflectance Spectroscopy: Principles, Methods, Applications*. [By] Gustav Kortüm. Translated from the German by James E. Lohr. With 160 Figures. Springer.
38. Khatoon, S., Coolahan, K., Lofland, S.E. and Ahmad, T., **2012**. Optical and magnetic properties of solid solutions of $In_{2-x}Mn_xO_3$ (0.05, 0.10 and 0.15) nanoparticles. *Journal of Alloys and Compounds, 545*, pp.162–167.
39. Liu, Y., Liu, P., Su, Z., Li, F. and Wen, F., **2008**. Attapulgite-Fe_3O_4 magnetic nanoparticles via co-precipitation technique. *Applied Surface Science, 255*(5), pp.2020–2025.
40. Papadas, I., Christodoulides, J.A., Kioseoglou, G. and Armatas, G.S., **2015**. A high surface area ordered mesoporous $BiFeO_3$ semiconductor with efficient water oxidation activity. *Journal of Materials Chemistry A, 3*(4), pp.1587–1593.
41. Gao, F., Chen, X., Yin, K., Dong, S., Ren, Z., Yuan, F., Yu, T., Zou, Z.G. and Liu, J.M., **2007**. Visible-light photocatalytic properties of weak magnetic $BiFeO_3$ nanoparticles. *Advanced Materials, 19*(19), pp.2889–2892.
42. Maxwell, J.C., **1973**. *Electricity and Magnetism*. London, Oxford University Press.
43. Wagner, K.W., **1993**. Zur theorie der unvoll kommener dielektrika. *Ann. Phys., 40*, pp.818–826.
44. Koops, C.G., **1951**. On the dispersion of resistivity and dielectric constant of some semiconductors at audio frequencies. *Physical Review, 83*(1), pp.121–124.
45. Jiang, Q.H., Liu, F.T., Nan, C.W., Lin, Y.H., Reece, M.J., Yan, H.X., Ning, H.P. and Shen, Z.J., **2009**. High-temperature ferroelectric phase transition observed in multiferroic $Bi_{0.91}La_{0.05}Tb_{0.04}FeO_3$. *Applied Physics Letters, 95*(1), p.012909.
46. Patil, D.R., Lokare, S.A., Devan, R.S., Chougule, S.S., Kanamadi, C.M., Kokekar, Y.D. and Chougule, B.K., **2007**. Studies on electrical

and dielectric properties of $Ba_{1-x}Sr_xTiO_3$. *Materials Chemistry and Physics, 104*(2–3), pp.254–257.

47. Catalan, G. and Scott, J.F., **2009**. Physics and applications of bismuth ferrite. *Advanced Materials, 21*(24), pp.2463–2485.

48. Palai, R., Katiyar, R.S., Schmid, H., Tissot, P., Clark, S.J., Robertson, J., Redfern, S.A.T., Catalan, G.A. and Scott, J.F., **2008**. β phase and γ-β metal-insulator transition in multiferroic $BiFeO_3$. *Physical Review B, 77*(1), p.014110.

49. Raymond, O., Font, R., Suarez-Almodovar, N., Portelles, J. and Siqueiros, J.M., **2005**. Frequency-temperature response of ferroelectromagnetic $Pb(Fe_{1/2}Nb_{1/2})O_3$ ceramics obtained by different precursors. Part I. structural and thermo-electrical characterization. *Journal of Applied Physics, 97*(8), p.084107.

Received: 17 December 2018. Accepted: 11 March 2019.